

Supplementary table 1. TLS formation and pathological characteristics of breast cancer.

Variables	Total	TLS formation		P
		Free/rare	Positive	
Age, years				
≤55	54	31	23	0.234
>55	47	21	26	
Tumor size (invasive area, median 2.6cm)				
≤2.6cm	50	29	21	0.234
>2.6cm	51	23	28	
Tumor type				
Luminal type	77	46	31	<b>0.001</b>
HER2 <sup>+</sup> type	14	6	8	
triple negative type	10	0	10	
Hormone receptor				
negative	18	3	15	<b>0.001</b>
positive	83	49	34	
Histological grade				
G1, G2	70	43	27	<b>0.005</b>
G3	31	9	22	
Nuclear grade				
G1, G2	67	41	26	<b>0.011</b>
G3	34	11	23	
% of invasive component				
0-25	14	7	7	0.062
26-50	9	8	1	
51-	78	37	41	
Lymphovascular invasion				
negative	74	40	34	0.501
positive	27	12	15	
Stage				
1A	59	31	28	0.846
2A	19	8	11	
2B	6	3	3	
3A	3	1	2	
3B	11	7	4	
3C	3	2	1	
Total		52	49	

Bold numbers indicate statistical significance.

Supplementary Table 2. Pathological evaluation of 20 breast cancer cases.

Patient ID	Age	Histological type	Histological grade	Nuclear grade	Invasive component %, size	Nuclear atypia	Structural atypia	Nuclear atypia	Number of mitotic figures (per 10 HPF)	HR	HER2	Ki67%	Stage
1	49	invasive ductal	3	3	90	2	3	2	5-10	positive	0	56.4	2B
2	61	invasive ductal	1	1	20	1	1	1	0-4	positive	1+	4.2	1A
3	59	invasive ductal	1	1	80	2	2	2	0-4	positive	0	10.0	3B
4	69	invasive ductal	1	1	100	2				positive	0	2.6	1A
5	38	invasive ductal	2	1	70	2	1	2	0-4	positive	1+	3.6	1A
6	55	invasive ductal	1	1	90	2	1	2	0-4	positive	2+	6.4	2A
7	59	invasive ductal	1	1	95	2	1	1	0-4	positive	1+	11.6	1A
8	44	invasive ductal	2	2	90	2	2	2	5-10	positive	0	21.8	3B
9	71	invasive lobular	1	1	90	1	2	2	0-4	positive	0	21.2	3C
10	40	invasive ductal	1	1	90	1	3	1	0-4	positive	1+	22.4	1A
11	39	invasive ductal	2	1	70	2	3	2	0-4	positive	1+	24.8	1A
12	59	invasive ductal	2	2	80	2	2	3	5-10	positive	1+	18.6	1A
13	52	invasive ductal	3	3	70	3	3	3	10<	positive	2+	41	3C
14	43	invasive ductal	3	3	60	3	2	3	10<	negative	1+	22.2	2B
15	64	invasive ductal	2	1	80	2	3	2	0-4	positive	3+	18.2	2A
16	55	invasive ductal	3	3	95	3	3	3	5-10	negative	3+	32.0	2A
17	66	invasive ductal	3	3	100	2				negative	0	69.6	1A
18	49	invasive ductal	3	3	90	3	2	2	5-10	negative	2+	53.2	2A
19	69	invasive ductal	1	1	100	2				positive	2+	7.4	1A
20	70	invasive ductal	2	2	80	2	3	3	5-10	positive	1+	13.8	1A

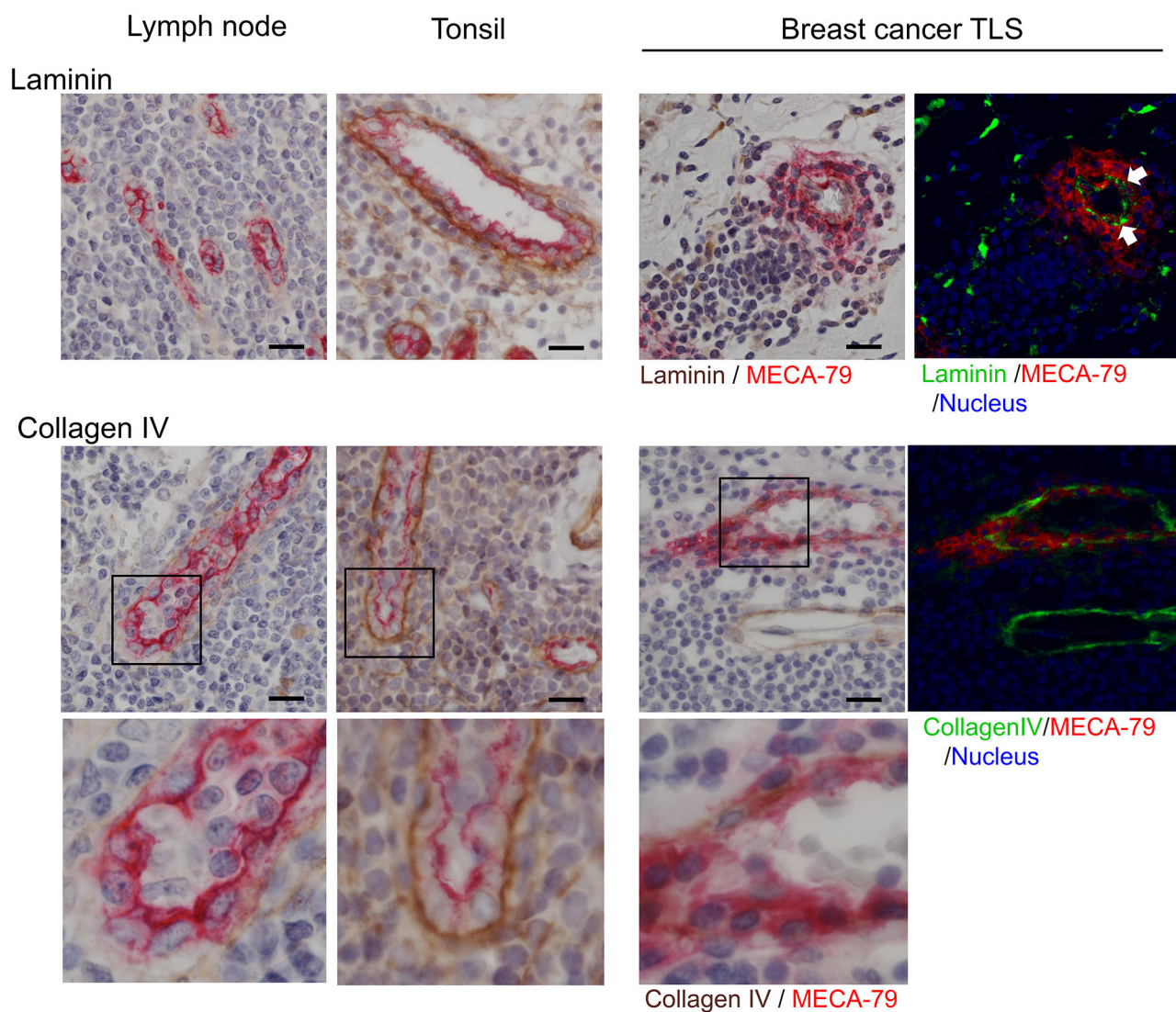


**Fig. S1 Immunostaining of secondary and tertiary lymphoid organs/structures.**

Immunohistochemistry of MECA-79 (red) with laminin or collagen IV (brown) to analyze HEVs of human lymph node, tonsil, and TLS of breast cancer. Nuclei are stained with hematoxylin (blue). Note thick area of MECA-79 staining around this tumor HEV (arrows). The right-most panels show color deconvolution of the images of cancer TLS, in which colors were reassigned as follows: laminin or collagen IV (green), MECA-79 (red), nuclei (blue). Scale bar, 200  $\mu$ m.

Lymph node

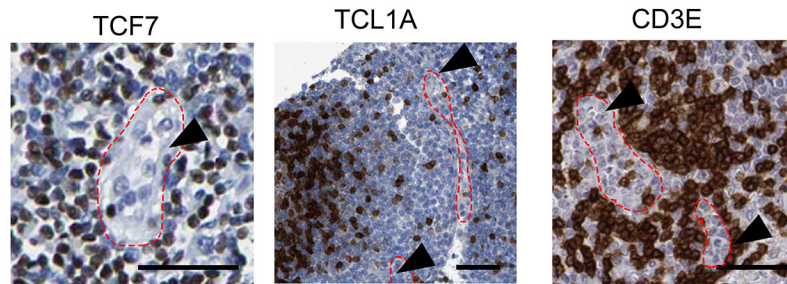


**Fig. S2 Immunostaining of lymph node in Human Protein Atlas.**

Images of immunohistochemistry staining of various proteins in human tissues (normal and cancer) are available at the Human Protein Atlas. Lymphocytes in normal lymph nodes were stained for TCF7, TCL1A, and CD3E (dark brown) with hematoxylin counterstaining (blue). HEVs are indicated by arrowheads with red dotted lines. Scale bar, 50  $\mu$ m.

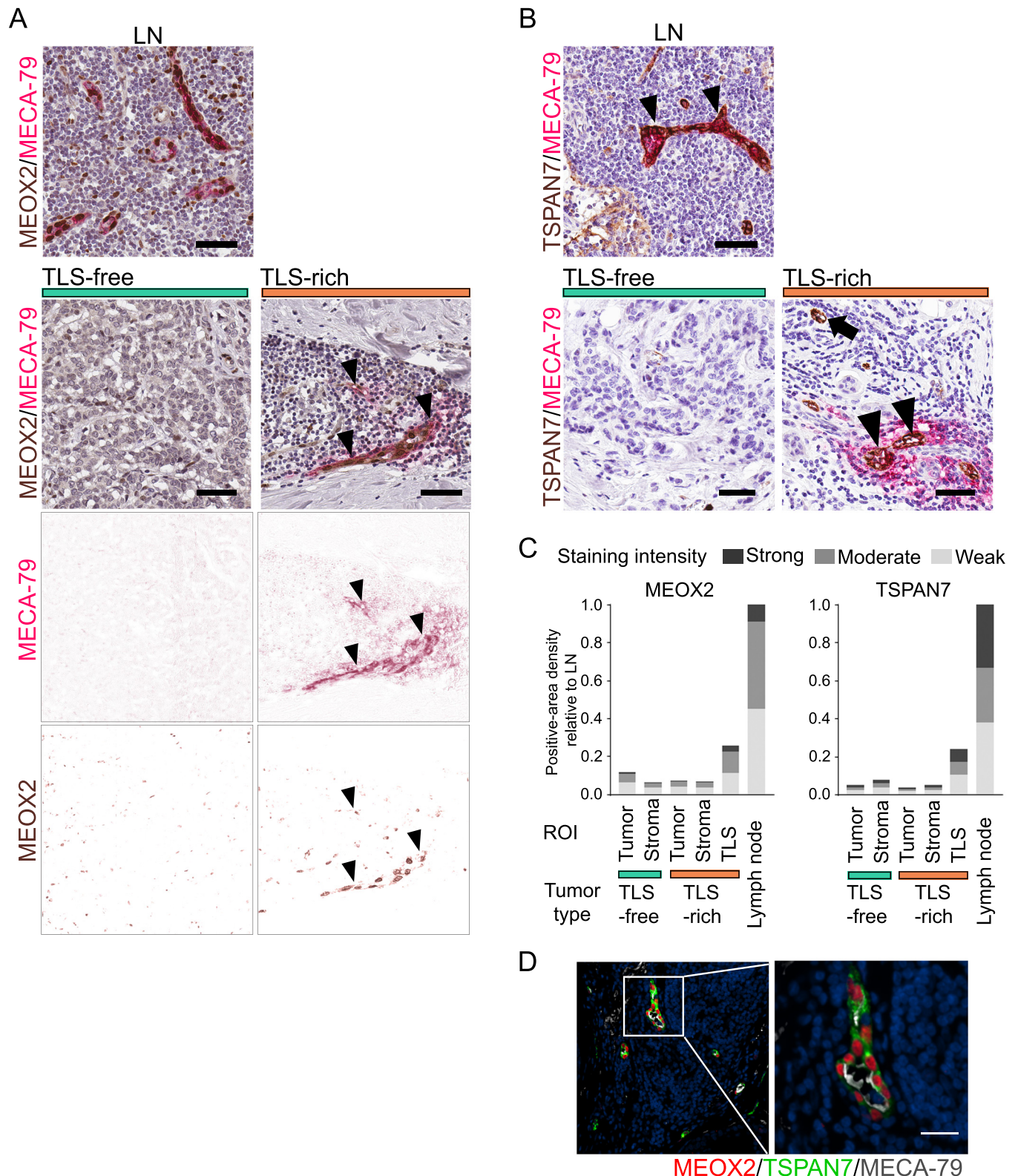


**Fig. S3 MEOX2 and TSPAN7 are highly expressed in breast cancer HEVs as well as lymph node.** (A and B) Histological sections were co-stained for MECA-79 and MEOX2 or TSPAN7 in TLS-rich (n=10) and TLS-free (n=10) breast cancer tissues and in the normal lymph node. Representative pictures were shown. The panel A also shows the images with color deconvolution to separate MECA-79 and MEOX2 signals. Scale bar, 50  $\mu$ m. Arrowheads in A; MECA-79<sup>+</sup>MEOX2<sup>+</sup> vessels. Arrowheads in B, MECA-79<sup>+</sup>TSPAN7<sup>+</sup> vessels. Arrow; MECA-79<sup>+</sup>TSPAN7<sup>+</sup> vessel. (C) The density of MEOX2<sup>+</sup> or TSPAN7<sup>+</sup> area in different tumor compartments (tumor parenchyma, stroma, and TLS) was determined from the immunostained tumor sections in (A) and (B), and compared with that of the normal lymph node (LN). The immunostaining of MEOX2 or TSPAN7 was categorized as strongly positive, moderately positive, and weakly positive in the graph. n=10(TLS-free), n=6(TLS-rich). (D) Immunofluorescence of HEVs in breast cancer TLS demonstrating co-expression of MEOX2, TSPAN7, and MECA-79. Scale bar, 20  $\mu$ m.

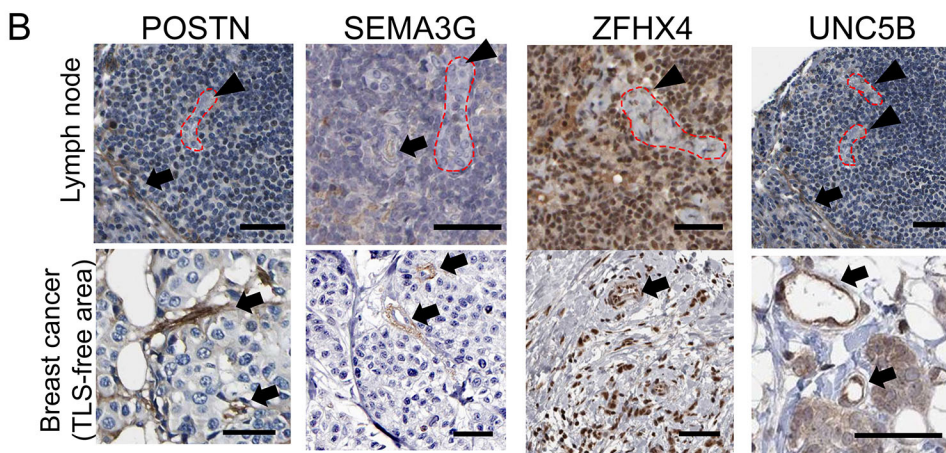
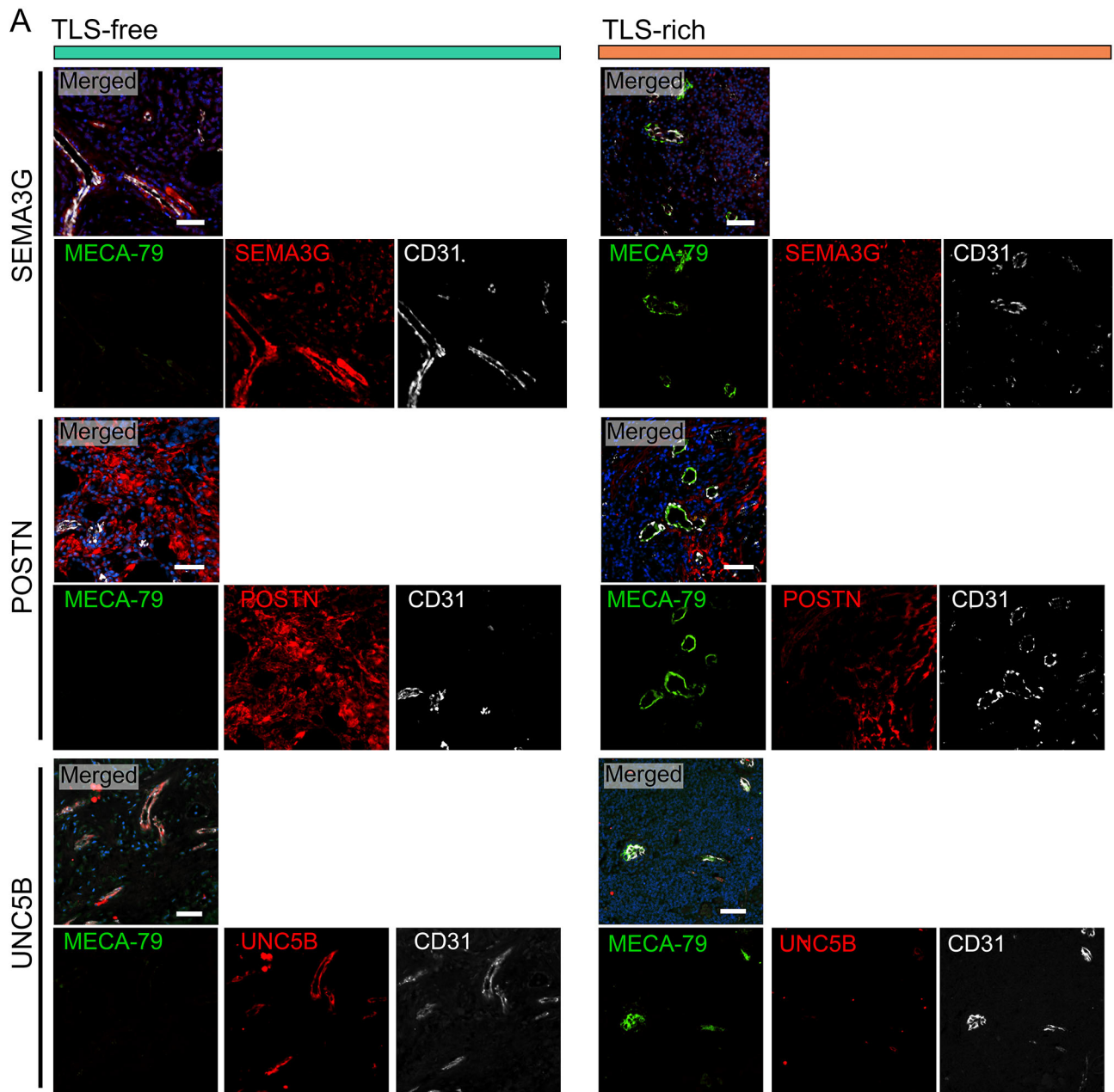


**Fig. S4 SEMA3G, POSTN, UNC5B, and ZFH4 are downregulated in tumor-associated HEVs.**  
 (A) Immunostaining of SEMA3G, POSTN, or UNC5B with CD31 and MECA-79 in TLS-free and TLS-rich tumors. Scale bar, 50  $\mu$ m. (B) Immunohistochemistry images of normal human lymph node and breast cancer tissues were obtained from Human Protein Atlas. The expression of SEMA3G, POSTN, UNC5B, or ZFH4 was analyzed in these tissues. Arrowheads, lymph node HEVs. Arrows, non-HEV blood vessels. Red dotted lines: HEVs. Scale bar, 50  $\mu$ m.

A

ID	Data set	Down	Up	Total	Method
BC This study	Human tumor-associated HEVs vs tumor vessels	41	35	76	This study: Laser Capture Microdissection & RNA-seq
LN 2014	Mouse peripheral lymph nodes HECs vs capillary ECs	465	570	1035	Microarray
LN 2019	Mouse peripheral lymph nodes homeostatic HECs vs capillary ECs	368	1189	1560	scRNA-seq
LN 2020	Mouse peripheral lymph nodes HECs vs non-HECs	309	235	544	scRNA-seq

B

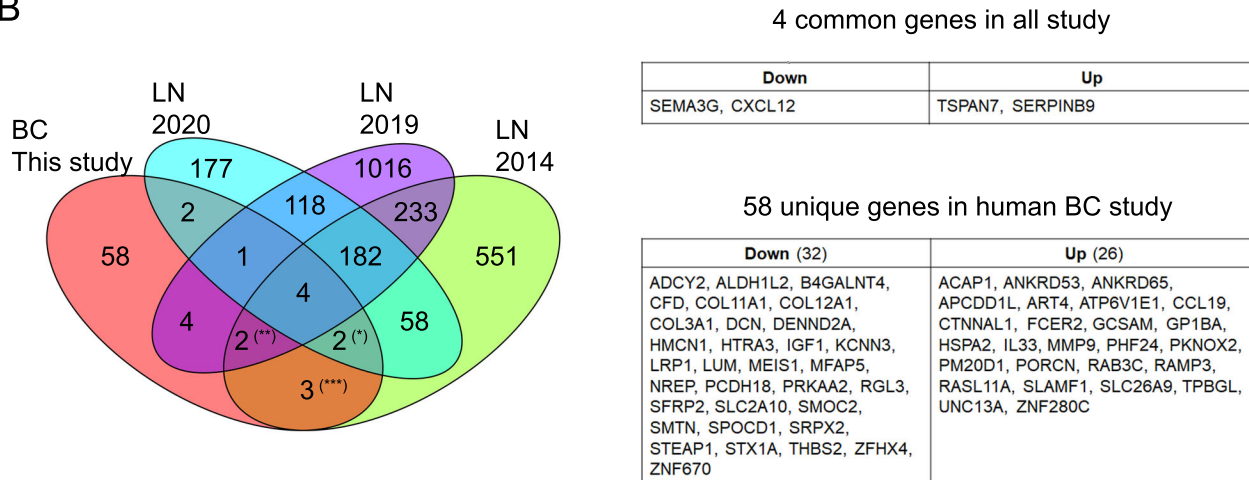


**Fig. S5 Comparison with previous transcriptome analyses.**

(A) List showing the data sets of the three studies used for this comparison. (B) Venn diagram shows four genes commonly upregulated or downregulated in HEVs compared with non-HEV vessels in all four studies. List of four genes which were found significantly up- or down-regulated in all studies. List of 58 differentially regulated genes (26 upregulated and 32 downregulated genes) in HEV vs. non-HEV tumor vessels that were not observed in the studies of mouse lymph node. Study ID: LN2014, Lee et al. (26); LN2019, Veerman et al. (25); LN2020, Brulois et al. (24). The differential expression of MEOX2 (\*), UNC5B (\*\*), POSTN (\*\*\*) were found in the indicated studies.

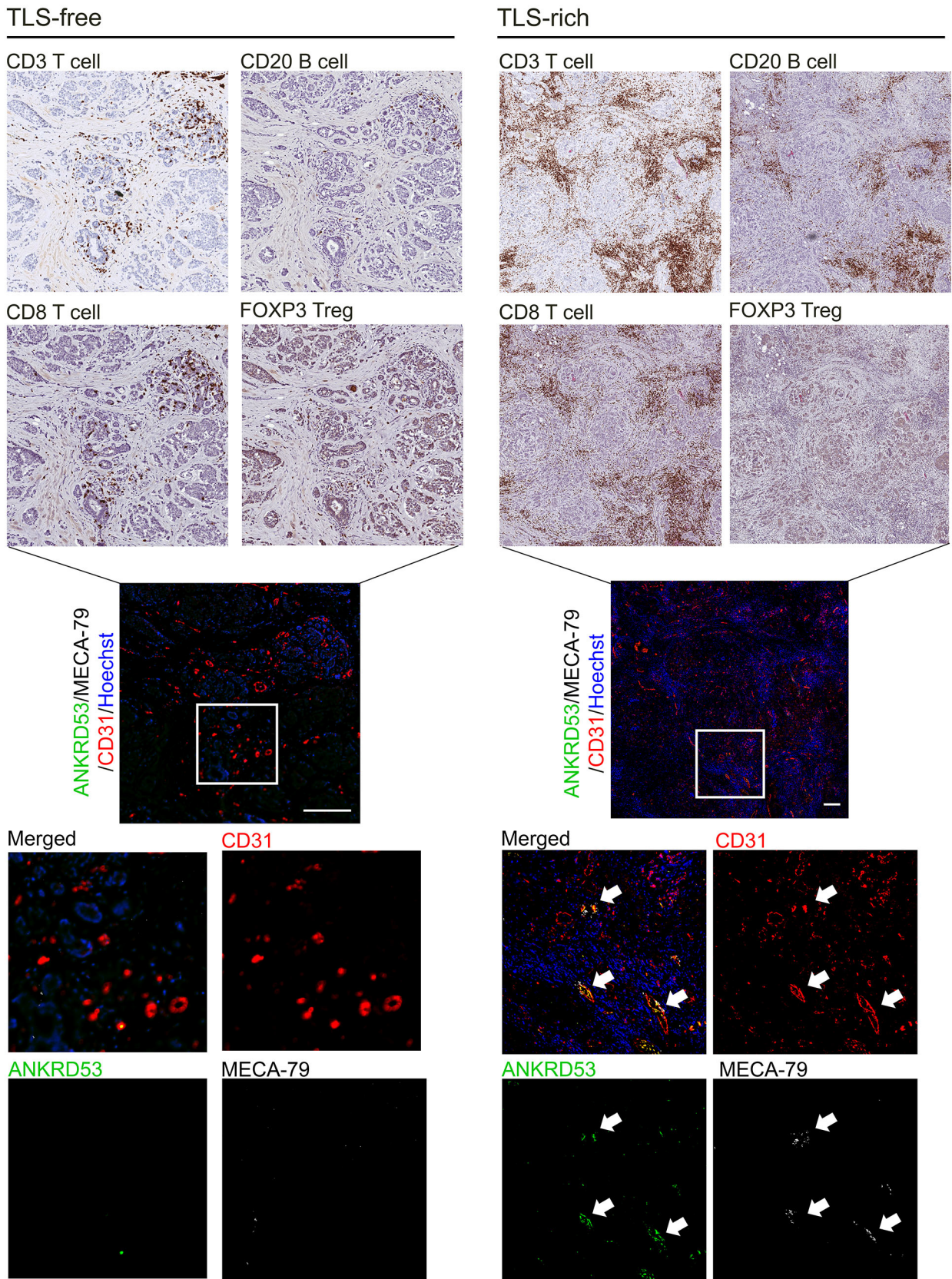


**Fig. S6 ANKRD53 is expressed by tumor-associated HEVs.**

Immunohistochemistry staining of different lymphocyte markers was conducted in serial tumor sections to visualize infiltration of T cells, B cells, and Treg cells in TLS-free and TLS-rich breast cancer (brown staining, upper panels). The consecutive sections of the same tumors were analyzed by immunofluorescence of ANKRD53, MECA-79, and CD31 (center and lower panels). Hoechst, nuclear staining (blue). Scale bar, 200  $\mu$ m. Areas in the white squares are enlarged in the lower panels.



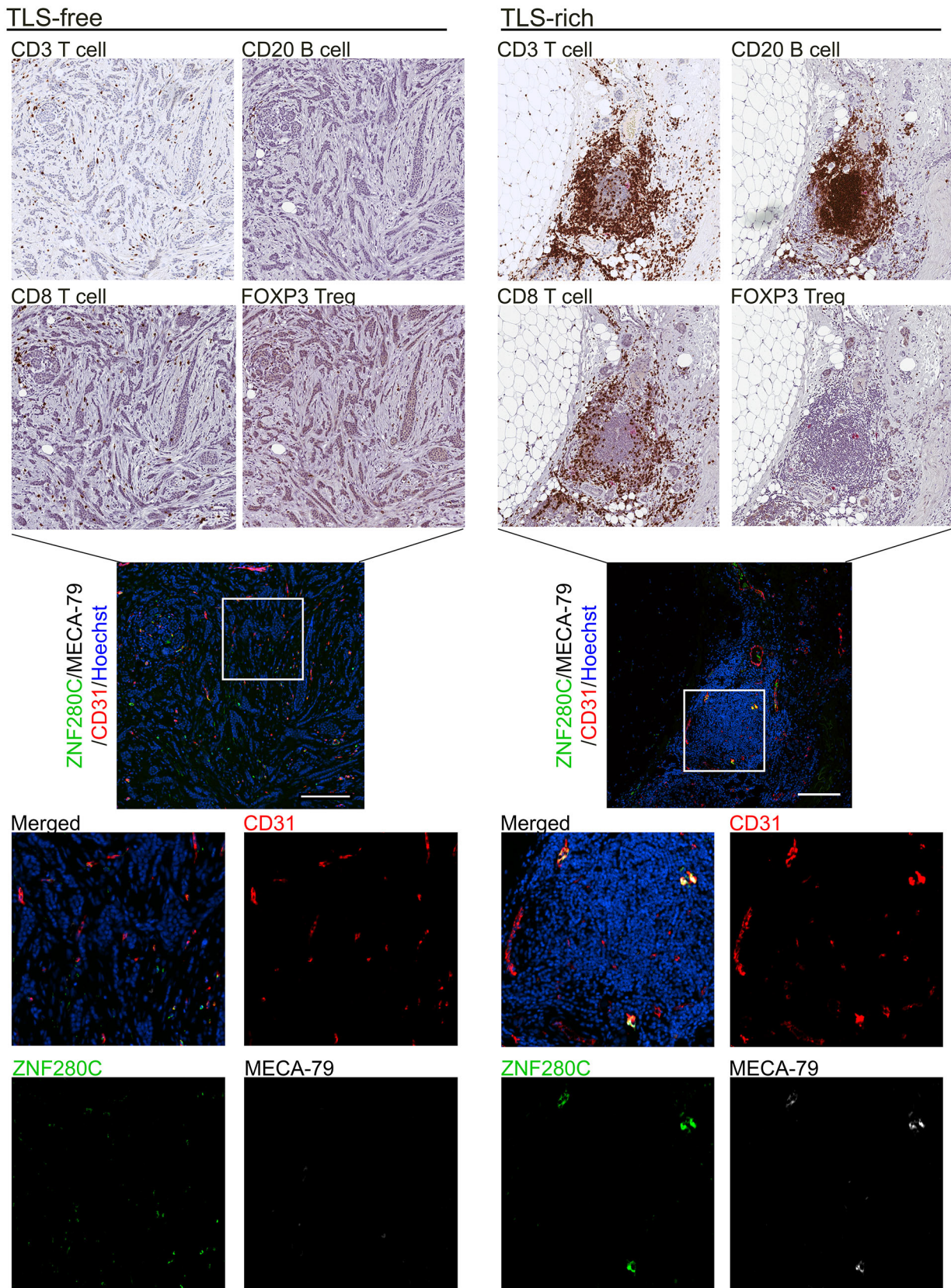


**Fig. S7 ZNF280C is expressed by tumor-associated HEVs.**

Immunohistochemistry staining of different lymphocyte markers was conducted in serial tumor sections to visualize infiltration of T cells, B cells, and Treg cells in TLS-free and TLS-rich breast cancer (brown staining, upper panels). The consecutive sections of the same tumors were analyzed by immunofluorescence of ZNF280C, MECA-79, and CD31 (center and lower panels). Hoechst, nuclear staining (blue). Scale bar, 200  $\mu$ m. Areas in the white squares are enlarged in the lower panels.

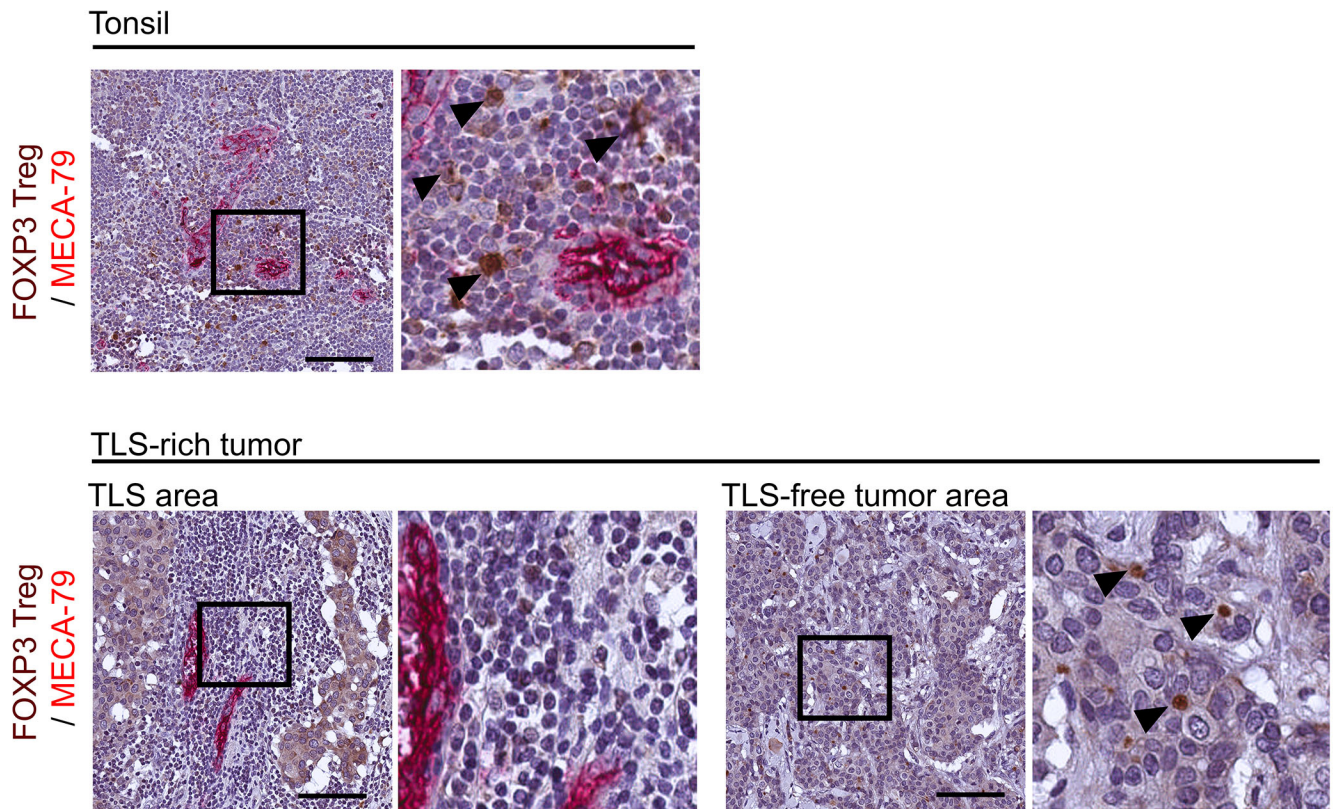
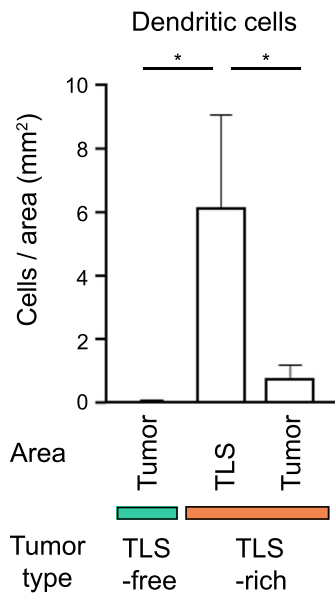


**Fig. S8 Treg in tonsil and TLS-rich breast cancer.**

FOXP3 staining of human tonsil and TLS-rich tumors from Fig. 6. The images of TLS and TLS-free area of the same tumor are shown in low and high magnification. Arrowhead, FOXP3<sup>+</sup> cells. Scale bar, 100  $\mu$ m.

A



B

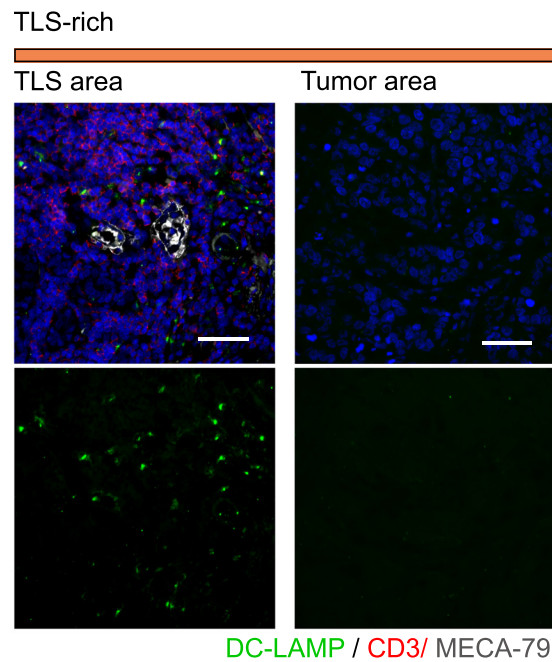


**Fig. S9 Accumulation of dendritic cells in TLS.**

(A) Dendritic cell (DC-LAMP<sup>+</sup> cell) density was analyzed in the TLS area and the tumor area of TLS-rich specimens, and the tumor area of TLS-free specimens. n=10(TLS-free), n=6(TLS-rich). \**P*<0.05. (B) Representative pictures of fluorescence staining for dendritic cells. Scale bar, 50  $\mu$ m.

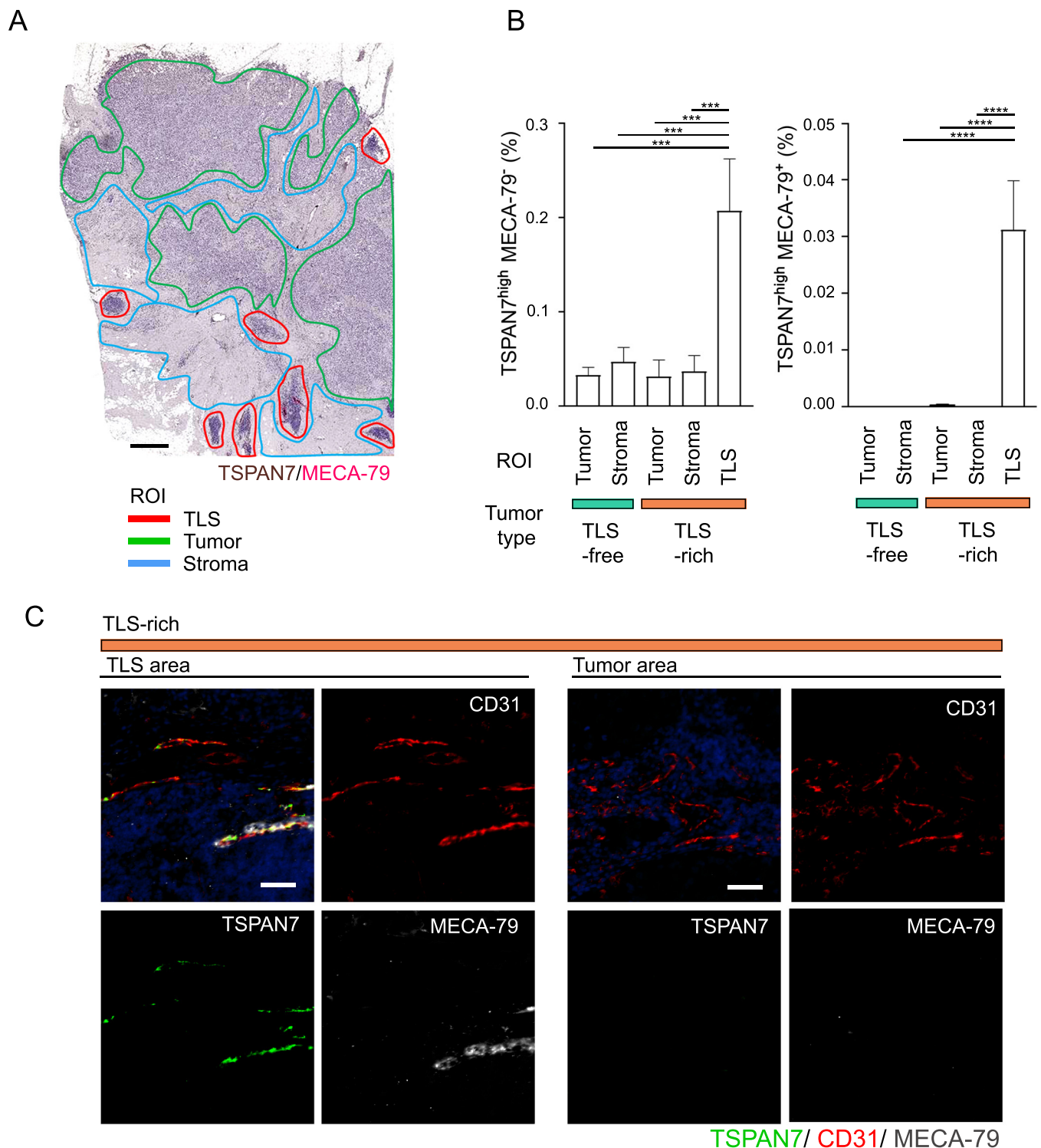


**Fig. S10 TSPAN7<sup>high</sup> MECA-79<sup>-</sup> blood vessels in TLS.**

(A) Representative image of TSPAN7 and MECA-79 immunostaining in a TLS-rich breast cancer specimen. Region of interest (ROI) for TLS area (red), tumor area (green), or stroma area (blue) was used to determine the density of TSPAN7<sup>high</sup> blood vessels in each area. Scale: 1 mm. (B) Vessel density (by area) of TSPAN7<sup>high</sup>MECA-79<sup>-</sup> or TSPAN7<sup>high</sup>MECA-79<sup>+</sup> vessels was determined in each ROI. TLS-free tumors, n=10. TLS-rich tumors, n=6. Data are presented as means ± SEM. \*\*\**P*<0.001, \*\*\*\**P*<0.0001. (C) Representative picture of a TLS-rich tumor with immunofluorescence staining for TSPAN7 (green), CD31 (red), MECA-79 (white), and Hoechst (blue). Scale: 50 μm.

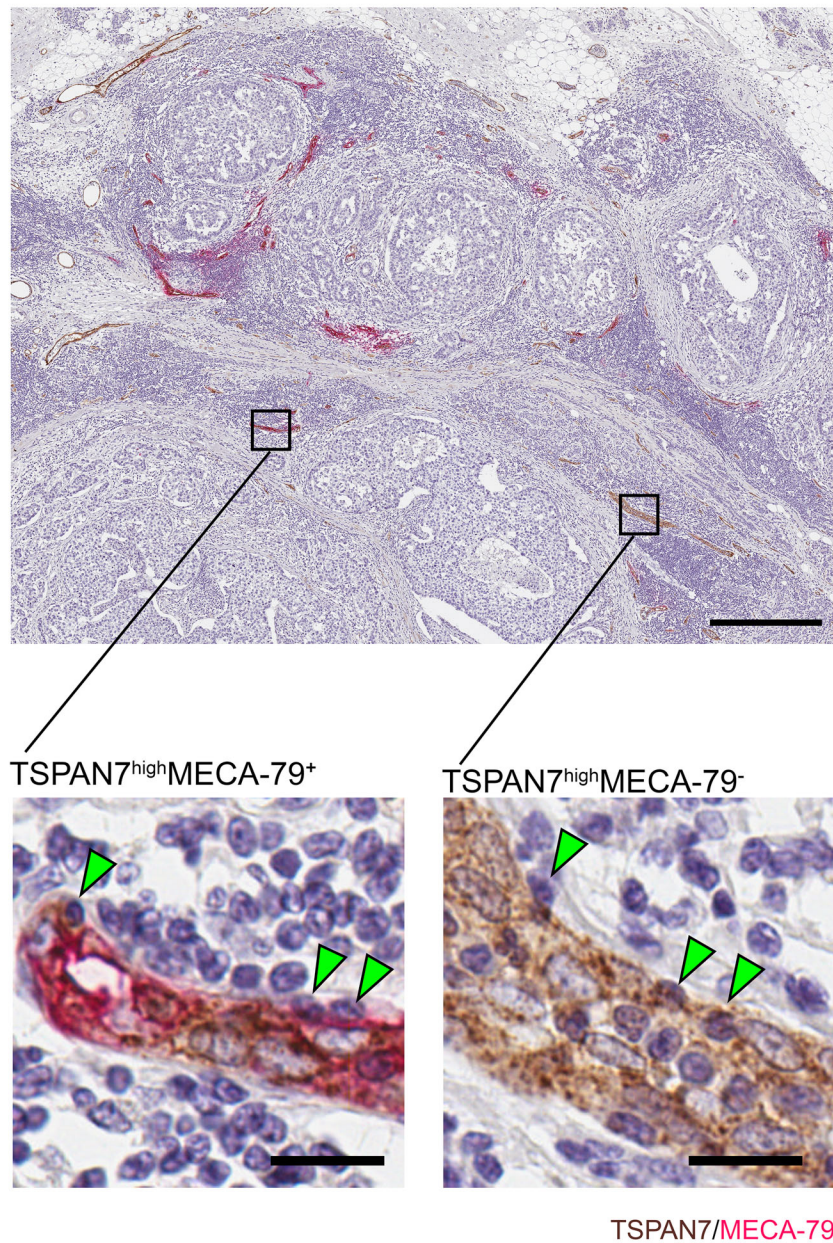


**Fig. S11 Leukocytes in endothelial wall.**

A low-magnification picture of MECA-79 (red) and TSPAN7 (brown) immunostaining of a TLS-rich breast cancer specimen is shown in the upper panel. Leukocytes engrafted in the endothelial wall of TSPAN7<sup>high</sup>MECA-79<sup>+</sup> and TSPAN7<sup>high</sup>MECA-79<sup>-</sup> blood vessels are shown in high-magnification pictures in the lower panels. Scale bar, 500  $\mu$ m for the upper panel; 20  $\mu$ m for lower panels.

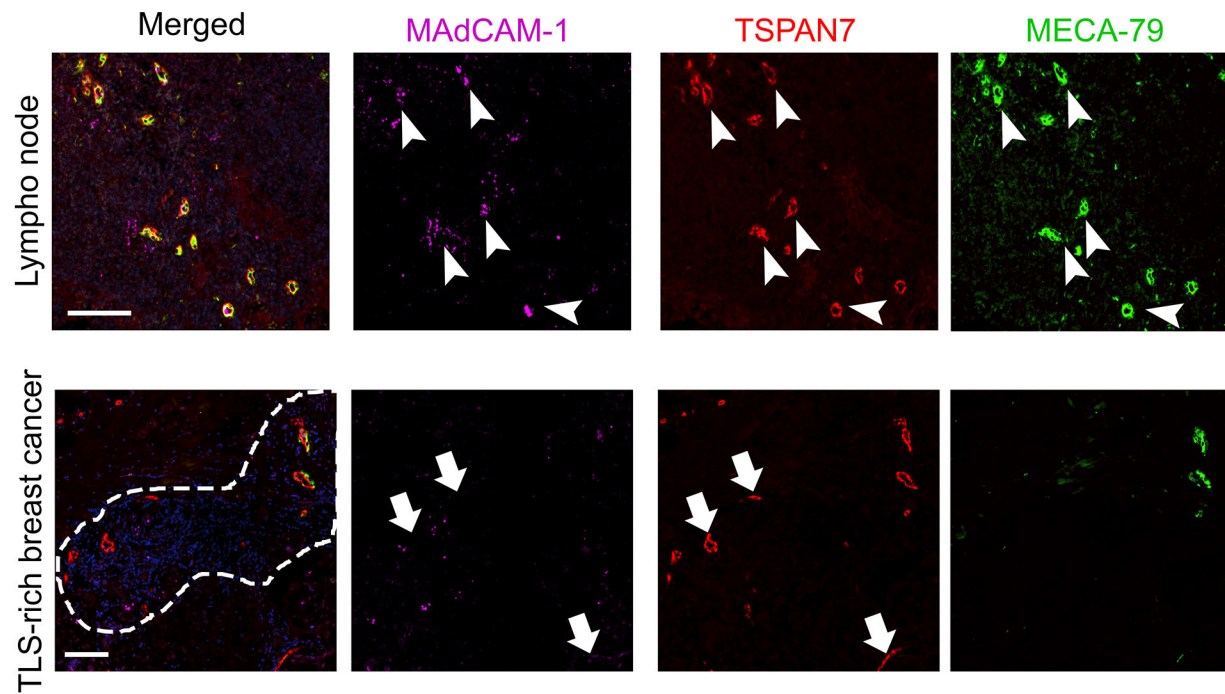


**Fig S12. Majority of tumor-associated HEVs are negative for MAdCAM-1 expression.**  
 Immunostaining of the normal lymph node and breast cancer TLS for MAdCAM-1. Arrowheads, TSPAN7<sup>+</sup>MECA79<sup>+</sup>MAdCAM-1<sup>+</sup> vessels. Arrows, TSPAN7<sup>+</sup>MECA79<sup>+</sup>MAdCAM-1<sup>-</sup> vessels. Representative pictures of lymph nodes and TLS-rich tumors are shown. n=5. The dashed line indicates TLS area. Scale bar, 100  $\mu$ m.